J Comp Physiol A (2005) 191: 157–174
DOI 10.1007/s00359-004-0581-9

ORIGINAL PAPER

Jacob L. Krans · William D. Chapple

The action of spike frequency adaptation in the postural motoneurons of hermit crab abdomen during the first phase of reflex activation

Received: 16 June 2004 / Revised: 6 October 2004 / Accepted: 20 October 2004 / Published online: 2 December 2004

Abstract Cuticular strain associated with support of the shell of the hermit crab, *Pagurus pollicarus*, by its abdomen activates mechanoreceptors that evoke a stereotyped reflex in postural motoneurons. This reflex consists of three phases: a brief high-frequency burst of motoneuron spikes, a pause, and a much longer duration but lower frequency period of spiking. These phases are correlated with a rapid increase in muscle force followed by a slight decline to a level of tone that is greater than that at rest but less than maximal. The present experiments address the mechanisms underlying the transition from the first to second phase of the reflex and their role in force generation. Although centrally generated inhibitory post-synaptic potentials (IPSPS) are present during the pause period of the reflex, intracellular current injection of motoneurons reveals a spike frequency adaptation that rapidly and substantially reduces motoneuron firing frequency and is unchanged in saline that reduces synaptic transmission. The adaptation is voltage sensitive and persists for several hundred milliseconds upon repolarization. Hyperpolarization partially restores the initial response of the motoneuron to depolarizing current. Spike frequency adaptation and synaptic inhibition are important mechanisms in the generation of force that maintains abdominal stiffness at a constant, submaximal level.

Keywords Crustacean · Reflex · Spike frequency adaptation · Motoneuron · Intrinsic

Abbreviations VSMN: Ventral superficial muscle motoneurons · PSDF: Probability spike density function · HCM: High Ca^{2+}, high Mg^{2+} Cole's saline · LCHM: Low Ca^{2+}, high Mg^{2+} Cole's saline

J. L. Krans (✉) · W. D. Chapple
Department of Physiology and Neurobiology,
University of Connecticut, 3107 Horsebarn Hill Rd.,
Storrs, CT 06269-4156, USA
E-mail: jacob.krans@uconn.edu
Tel.: +1-860-4863338

Introduction

Adult aquatic hermit crabs, *Pagurus pollicarus*, live in gastropod shells that exert five to ten times the downward force of the animal itself. The hydrostatic and decalcified abdomen of the crab supports the shell's weight above the ocean floor during common behaviors such as locomotion and interaction with other animals. Shell support is accomplished in part through the modulation of motoneuron spike rate to the superficial muscles of the abdomen as a function of load (Chapple 1973a, b). The ventral superficial muscles (VSM), those that contact the inner columella of the shell, are a primary element of this load compensation (Chapple 1973b). The motoneurons that innervate these postural muscles are activated by afferent activity in a stereotyped three-phase pattern (the tri-phasic reflex) and this reflex utilizes feedforward control (Chapple and Krans 2004). The neural connectivity and cellular attributes that contribute to the control of this reflex have not been described in detail. The present experiments examine the termination of the first phase of reflex activation, revealing sources of control that are intrinsic as well as presynaptic to the postural motoneurons.

Recent investigations of motoneuron and premotor control elements illustrate several sources of flexibility not considered in earlier studies (Binder et al. 1996). The action of intrinsic motoneuron properties in modifying premotor signals is an area of research that remains heavily investigated. Intrinsic membrane properties have been described across a broad range of species and are a major source of modulating the final motor pattern (mammals: Heckman et al. 2003; Lee et al. 2003; Prather et al. 2002; turtle: Alaburda et al. 2002; lamprey: Grillner et al. 1995; Parker 2003; stick insect: Gabriel et al. 2003; crustacea: Harris-Warrick 2002). The number of examples of intrinsic mechanisms described in motor systems has grown rapidly in recent years, and we are beginning to understand the significance of these elements in forming the final motor pattern. Much of the research on

intrinsic membrane properties has occurred in preparations with rhythmic activity. The action of intrinsic properties in tonic systems, and the influence of these actions on force generation are still not well understood and have not been as intensively examined. This is due in part to methodological restrictions in several preparations in which motoneurons are recorded (Magarinos-Ascone et al. 1999).

Force generation can be quantitatively investigated in the reflex control system of the hermit crab abdomen through the recording and manipulation of motoneurons and premotor neurons. Results from this type of investigation are readily associated with the maintenance of abdominal position; the hermit crab continuously supports its shell above the ocean floor. A recent characterization showed that the reflex activation of postural motoneurons in the hermit crab consists of three phases: phase 1 is 50–100 ms of robust monosynaptic and polysynaptic depolarization, phase 2 is a transient inhibition comparable to phase 1 in duration, and phase 3 is a much longer period of moderate excitation (Chapple and Krans 2004). The excitatory potentials characteristic of phase 1 generate average spike frequencies in the ventral superficial muscle motoneurons (VSMN) that are as much as fifty times greater than tonic firing. Force is generated rapidly in the VSM during the first phase of reflex activation.

The relationship between rate and contractile properties in crustacean muscles has recently been considered in more quantitative detail than was previously possible (Morris and Hooper 1997, 1998; Msghina et al. 1998). Consistent with observations made in these investigations, the present experiments suggest that force production in *Pagurus* ventral superficial muscles is well correlated with motoneuron frequency when burst duration is limited to 100 ms (phase 1 duration). In non-spiking muscles, such as the postural muscle of the hermit crab, the summation of excitatory junction potentials (EJP) dictates force generation (Atwood 1967). In contrast to spiking muscle, maximum depolarization of non-spiking muscle occurs only with sufficient temporal summation of EJPs (Jorge-Rivera et al. 1998). This property necessitates high-frequency motoneuron spiking to compensate for rapid disturbances.

In the intact hermit crab, force generated by the superficial muscles is modulated with changes in shell loading (Chapple 1973a, 1974, 1997). Reflex-generated forces are typically a small proportion of total available force (Chapple and Krans 2004). This is due to the reduction of motoneuron firing rate from the initial high-frequency of phase 1 that is necessary for rapid force generation. The mechanisms of this spike-rate reduction remain unknown. The rate of decay observed during the first phase that transitions into the cessation of firing that is characteristic of the second phase could be achieved either through local inhibitory feedback or an intrinsic spike-rate reduction mechanism. An intrinsic spike-frequency adaptation that acts during the brief initial phase of reflex activation in hermit crab is described in this report. This form of motoneuron spike rate modulation has been reported across a wide range of species, suggesting its relevance as a common means of modulation in motor control (mammal: Magarinos-Ascone et al. 1999; Sawczuk et al. 1995b; lamprey: Martin 2002; stick insect: Schmidt et al. 2001; Aplysia: Lewis et al. 1986).

Peak and average probability of VSMN rates vary little in response to widely varied afferent firing rates during phase 1 reflex activation (Chapple and Krans 2004). The range of motoneuron firing frequency was approximately an order of magnitude less than the range of afferent activity, but the two were strongly correlated. The peak and average probability of firing were used to describe motoneuron activity across each phase of the reflex in previous reports. An evaluation of changes in VSMN instantaneous frequency during phase 1 is presented here. Do changes in motoneuron frequency during phase 1 contribute to final abdominal tone? What is the relationship between the mechanism responsible for change in spike rate, the actual change in rate, and the final generation of force?

The present experiments investigate the mechanisms involved in the termination of the initial reflex phase in the postural motoneurons. The phase 1 burst activates an intrinsic membrane mechanism that profoundly reduces spike rate within the first 100 ms of spiking. We propose that, in addition to the centrally generated inhibitory post-synaptic potentials (IPSPS) of phase 2, phase 1 is terminated in part by this frequency adaptation. Once activated, the mechanism responsible for frequency reduction lasts several hundred milliseconds, probably acting throughout the next two phases of the reflex. The action of motoneuron rate reduction during phase 1 is also evaluated at the level of force generation in the postural muscle. We propose that the cessation of phase 1 is critical to the modulation of force; sustained spike rates similar to those observed early in phase 1 would rapidly recruit maximal force, leaving no range for modulation. These results support the hypothesis that the shaping of the tri-phasic reflex requires a coordinated contribution from both presynaptic elements and intrinsic membrane properties.

Methods

Collection and maintenance

Pagurus pollicarus was collected from sublittoral areas in Fishers Island Sound off the central coast of Connecticut. The crabs were kept in a 12/12 light cycle environmental room at 10°C in filtered tanks of artificial seawater (Instant Ocean, Aquarium Systems, Inc, Mentor, OH, USA).

Dissection

After separating the thorax from the abdomen, the posterior abdomen was exposed with a longitudinal

incision along its medial dorsal surface, which preserved the ventral musculature. The hepatopancreas and the large fast flexor muscles of the third, fourth, and fifth segments were removed, exposing the abdominal nervous system. The first ganglionic roots, containing the majority of mechanoreceptor afferents of the segment, were exposed laterally by removing the overlying longitudinal muscle fibers of the next more rostral segment. A rendering of the superficial anatomy of the abdomen is shown in Fig. 1a. Most experiments were performed on the fourth ganglion, which is similar in motor output to the other abdominal ganglia. The right first root was preferentially used for afferent stimulation experiments; it is composed almost entirely of sensory afferents. Two preparations were used: (1) the isolated abdominal nerve cord, consisting of all abdominal ganglia. In this preparation, all peripheral nerves were cut except for one motor root (third root) of the fourth ganglion. The afferent nerve was cut distally and drawn into a suction electrode for electrical stimulation. In experiments where force measurements were not necessary, the motor root was cut distally and potentials were recorded with a suction electrode, (2) the fourth ganglion was physically isolated by severing the 3–4 and 4–5 connectives close to the third and fifth ganglia (Fig. 1b). The recording and stimulation procedures were the same as in (1). In both preparations, the fourth ganglion was mechanically desheathed for intracellular recording.

Fig. 1 Schematic of the preparation. **a** Superficial structures of *Pagurus* abdomen, caudal most portions are positioned in the *bottom left corner*, right side is thus shown on the right of the rendering (after Chapple 1969). The ventral nerve cord runs along the longitudinal center of the image. Portions used in experiments discussed herein are in *black*. Tabs glued to the cuticular surface (not to muscle layer directly) for measurement of force are shown in *gray* with black perimeters. *Scale bar*: 5 mm. **b** One ganglion of the abdominal nerve cord is shown in *gray*. At *far right* is the extracellular electrode used for stimulus to the first nerve (afferent stimulus) and the hook electrode used to record these potentials. The intracellular VSMN electrode is positioned in the neuropil of the ganglion, and the extracellular suction electrode (*en passant*) is positioned peripherally at the third nerve (second nerve not shown). Elements of the schematic may not be to scale, *bar*: 2 mm

Solutions and data acquisition

The preparations were maintained at 12.5°C in Cole's solution (in mM/l): NaCl 460, KCl 15.7, $CaCl_2$ 25.9, $MgCl_2.6H_2O$ 8.3, Na_2SO_4 8.4, buffered with HEPES to pH 7.4. A high Ca^{2+}, Mg^{2+} saline (HCM) was used in some experiments: NaCl 408.7, KCl 15.7, $CaCl_2$ 64.75, $MgCl_2.6H_2O$ 20.75, Na_2SO_4 8.4. A lowered Ca^{2+} and elevated Mg^{2+} saline (LCHM) was also used in some experiments: NaCl 408.7, KCl 15.7, $CaCl_2$ 13.0, $MgCl_2.6H_2O$ 20.75, Na_2SO_4 8.4

Extracellular potentials from the motor nerve were recorded either with polyethylene or glass suction electrodes. A hook electrode was used in some experiments to record potentials in the afferent root after electrical stimulation (Fig. 1b). Signals were amplified with an A-M Systems differential AC amplifier with a passband of 10 Hz to 1 kHz and digitized at 5 kHz with user-composed routines and a CED Power 1401 Data Acquisition system (Spike 2 and Signal software, Cambridge Electronic Design, Cambridge, England). Intracellular recordings were made with 40–80 MΩ glass micropipettes filled with 2 M potassium acetate, using an AxoClamp 2B amplifier. Intracellular recordings were made from the third, fourth, and fifth abdominal ganglia to ensure that results were general to these central ganglia, though the majority of analysis was done using data collected in the fourth ganglion. All intracellular recordings were made in bridge mode. Multi-step protocols were executed using DAC outputs on the CED 1401 and the AxoClamp 2B.

To record forces generated by the longitudinal layer of the VSM, a force transducer was attached to plates glued to the cuticle of the third and fifth right segments (Fig. 1a). The left VSM and motor root were removed and the right VSM and motor root were left intact. A pseudorandom number table was generated using Matlab (The MathWorks, Inc, Natick, MA, USA) and used to order the intensities of electrical stimuli to the afferent root, as well as current steps to VMSN. There were between 10 and 30 repetitions of each experimental manipulation. For these repetitions, the intertrial pause was varied randomly about a mean value of 55 s. This duration was sufficiently long for both tonic and phasic behavior of the motoneurons to return to a stable baseline and for muscle tone to return to a stable base-

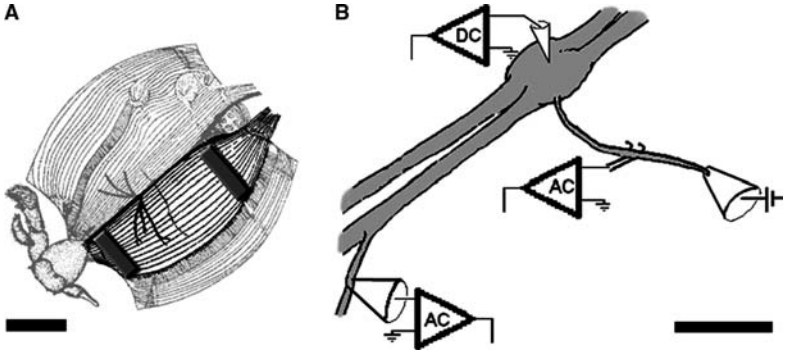

line value (data not shown). In experiments of depolarizing current injection, the number of spikes per trial was typically greater than 20, and over a minimum of ten repetitions, this gave minimum spike counts well into the hundreds. A predominate metric of the report is based on instantaneous frequency, for which the number of observations is simply spike count minus one, and was always between 200 and 3,000 per preparation.

Criteria for intracellular identification of the VSMN have been described in detail previously (Chapple and Krans 2004). Briefly, four main criteria were used: (1) orthodromic action potentials in the intracellular record were correlated 1:1 with an extracellular action potential in the motor root, (2) antidromic stimulation of the motor root produced an intracellular action potential that followed electrical stimulus to >90 Hz without changes in the latency of the action potential, (3) in several experiments, identification of the motoneurons was confirmed via intracellular recordings of muscle junction potentials that were correlated to potentials in the motor root, and (4) extracellular amplitude ratios between the motoneurons of the third ganglionic roots from the third, fourth, and fifth ganglia were also used, as previously described (Chapple and Krans 2004). Finally, tonic frequency and the response to reflex activation were additional criteria for identifying the motoneurons, as these are consistent and unique to individual motoneurons.

Data from intracellular recordings in which current polarity and magnitude were utilized as an approximation of membrane potential level were judged acceptable for analysis if the following criteria were met: (1) progressive depolarization, via current injection, gave rise to progressively smaller action potential voltage deflections, (2) average latency to the first spike, upon injection of the maximum depolarizing current used in any given experiment, was less than 20 ms, and (3) hyperpolarizing current was sufficient to abolish spiking due to afferent activation.

Data analysis

Records of extracellular spike trains, intracellular membrane potentials, and force traces were displayed and analyzed with Matlab (The MathWorks, Inc, Natick, MA, USA). For extracellular potentials, a threshold was set visually so that the peak-to-peak amplitudes (maximum positive excursion plus the maximum negative excursion) and spike times (measured from a positive to negative zero crossing) for all spikes above that threshold could be recorded in a table. An amplitude histogram of all the spikes for the nerve in an experimental file (typically consisting of 20 repetitions) was constructed and the lower and upper boundaries for a desired peak selected to define a single motor unit. Once concatenated, individual spike times and amplitudes were saved for further analysis.

Instantaneous frequency values represent the inverse of the interval between two discrete spike times. In order to display these graphically as a function of time, each instantaneous frequency value was given one discrete time of occurrence by finding the midpoint in time between the two times of the spikes used in its computation $[(t_{i+1}-t_i)/2]$.

As described in previous reports from our laboratory, we have chosen to use the probability spike density function (PSDF) as a means of providing a continuous approximation of spike rate probability computed from numerous repetitions of an experimental design. The PSDF provides a smooth function that is useful in identifying gross changes in spike pattern and rate. The sampling window of spike times used in these computations was 10 ms and the standard deviation of the Gaussian kernel with which spike data were convolved was 50 ms. While these parameters attenuate high spike rates, the function provides a useful graphical display of the three phases of the reflex discussed herein.

Ratio values of two spike frequencies are used as a metric often in this report. This ratio represents the quotient of two distributions of interspike interval times. A standard formula for fractional uncertainty was used for ratio values (Taylor 1982). The distribution of computed ratios is partially dependant on inter-preparation changes in the level of activity of motoneurons investigated. All other means are reported as mean ± standard error of the mean unless otherwise noted.

Results

Activation of mechanoreceptors or electrical stimulation of their axons elicits a stereotyped reflex activation of VSMN, the tri-phasic reflex, which is produced by several different classes of excitatory post-synaptic potentials (EPSPS) and at least one class of IPSPS (Chapple and Krans 2004), indicating that numerous premotor elements are involved in the tri-phasic reflex. Although all necessary neural elements that generate the three reflex phases are present in the physically isolated abdominal ganglion, the underlying mechanisms of these components are unknown. The present experiments are directed toward understanding the properties of the first phase, a burst of motoneuron spikes. This phase is the briefest of the three, lasting between 50 and 100 ms. It is much less variable, both in its average and peak frequencies, than the two later components of the reflex (Chapple and Krans 2004), and individual motoneurons may fire at frequencies of several hundred pulses per second (PPS).

Reflex activation

Electrical stimulation of the right first ganglionic root, which is made up primarily of sensory fibers, generates the tri-phasic reflex (Chapple and Krans 2004). By stimulating the nerve at a distal location, afferent

potentials can be recorded at a site more proximal to the ganglion (Fig. 2a), showing that a single afferent action potential is sufficient to trigger the tri-phasic reflex, which lasts several seconds. Figure 2b is a typical extracellular recording from the motor root (third ganglionic root) and depicts the three phases of reflex activation. The general form of the tri-phasic reflex is observed in all VSMN, though each is activated in a slightly different manner. An averaged response, displayed in a PSDF (Fig. 2c) shows these phases in three of the six VSMN of the right side of the fourth abdominal segment. The motoneurons first fire a burst of action potentials (phase 1), the spike rate is then reduced to sub-tonic levels (phase 2), and finally the spike rate is elevated to supratonic levels that are less than those of the initial burst (phase 3).

Two examples of VSMN spike frequency, recorded intracellularly during phase 1, are shown in Fig. 2d. The uppermost portions of each panel in Fig. 2d show extracellular recordings from the motor root, to which the intracellular spikes below are correlated. Instantaneous frequency was computed from intracellular spike times to quantify the change in rate over the brief motoneuron burst of phase 1. The transition between phase 1 and phase 2 is characterized by a smooth decay in frequency, a concurrent repolarization of the membrane potential, and the advent of IPSPS with latencies after afferent activation of 50–100 ms. The left panel illustrates the decay in spike rate observed during phase 1 when no apparent IPSPS occur during the first 80 ms of activation. The right panel shows the transient reduction in spike rate when a putative IPSP occurs at about 60 ms poststimulus.

Inhibitory post-synaptic potentials that arrive late in phase 1 act to rapidly reduce phase 1 spike frequency (Fig. 2d), but the excitatory potentials driving motoneuron depolarization are obscured during this period of spiking. This initial synaptic depolarization is critical in characterizing the change in spike rate during phase 1. Figure 3a is an intracellular recording from VSMN when an afferent stimulus was delivered during hyperpolarization. No action potentials occurred during the period of hyperpolarization, and the compound EPSP that immediately follows afferent stimulus is approximately three times larger than single spontaneous EPSPS recorded during hyperpolarization. These evoked potentials amidst hyperpolarization are typically greater than the spike amplitude observed during tonic firing. This suggests that the location of intracellular recording is electrotonically distant from the spike initiation zone, and that the recording site may be located in the dendritic portion of the motoneuron.

Phase 1 premotor synaptic content (EPSPS)

The voltage decay of the evoked potential illustrated by Fig. 3a could be generated by a decrease in the amplitude and number of synaptic potentials or by a combination of pre and postsynaptic mechanisms. We measured the amplitudes of post-synaptic potentials in VSMN when electrically stimulating the afferent root with 1-s trains at about 15 Hz (Fig. 3b). VSMN were hyperpolarized for these experiments to eliminate spiking. Amplitudes of the ensuing voltage deflections were binned (1 mV) and displayed in histogram form (Fig. 3c). In this recording from the medial VSMN, the deflections could be divided into four distributions with means of 4.26 ± 0.26, 10.17 ± 0.32, 16.53 ± 0.18, and 23.08 ± 0.45 mV. Individual EPSP amplitudes from each of the distributions were chronologically interspersed throughout the stimulus period and did not noticeably change in amplitude (Fig. 3b). The mean amplitudes of each of the three larger distributions were similar to values predicted by computing multiples of the smallest amplitude. Predicted values for 2×, 4×, and 8× the mean amplitude of the smallest observed deflection were 8.53, 17.05, and 25.58 mV, respectively. There was no obvious increase or decrease in the difference between predicted and observed values, nor was there a time dependent change in post-synaptic potential amplitude (Fig. 3b). Variation in the conduction velocity of several afferent axons would produce an initial depolarization that is a compound event consisting of several EPSPS of similar amplitude arriving closely in time (Chapple 2002).

Excitatory post-synaptic potentials that are characteristic of phase 1 arrive at a higher frequency than the stimulus frequency described above: 15 Hz (Fig. 3a, inset). In the medial and lateral VSMN, the interval between the stimulus artifact and the first peak of the evoked potential was 23.2 ± 0.62 ms ($n = 4$ VSMN). The next interval, between the first and second peaks of the initial evoked potential, was more variable and longer: 36.8 ± 2.37 ms ($n = 4$ VSMN; Fig. 3a). To achieve intervals similar to these while using electrical stimulus of the afferent nerve, brief trains of stimuli between 25 and 40 Hz were delivered to the afferent nerve. Figure 3d is an averaged trace ($n = 20$) from one series of these experiments in the lateral VSMN. The first peak of depolarization did not vary in amplitude during different trials. Later portions of the averaged record show decreases in EPSP amplitude due to the progressive asynchrony of EPSPS in different trials. After about the first 300 ms, the averaged record shows a relatively constant depolarization that does not adapt over the duration investigated (time $\leq$ 2 s, Fig. 3d). These results indicate that during phase 1 there is a transient repolarization of the membrane potential following the initial evoked potential, that thereafter the membrane potential remains depolarized relative to rest, and that there is no obvious facilitation or depression of EPSPS.

Motoneuron spike rate reduction phenomenon

Figure 4 shows that spike frequency adaptation of VSMN when synaptically activated and when depolar-

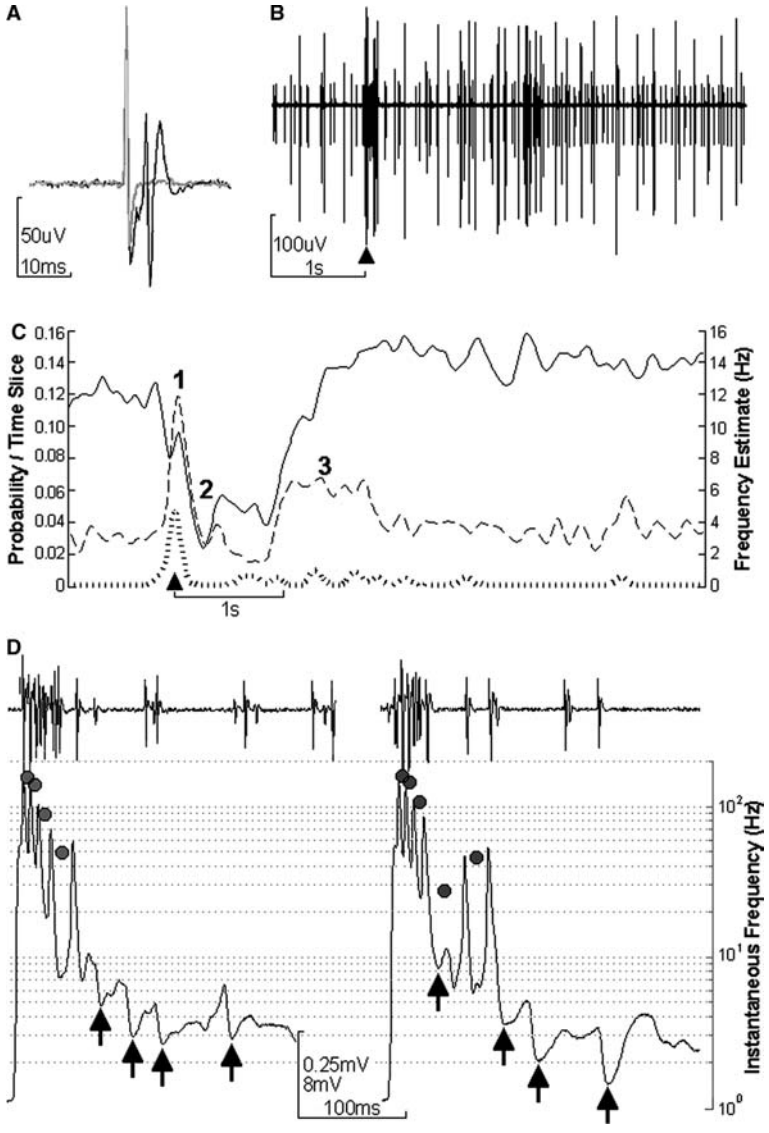

ized by passing intracellular current is similar in amplitude and time course. Figure 4a illustrates the rate reduction of three VSMN after a single electrical stimulus is delivered to the afferent root (in eight preparations, the stimulus was delivered for a minimum of ten repetitions). In these experiments, frequency adaptation could be adequately fit by either a first or second order exponential; there is considerable variability that increases with time after stimulation of the afferent root (F test for first and second order approximations: $P < 0.01$, each). This variability can be partially attributed to the slightly sporadic timing of post-synaptic potentials previously described (Chapple and Krans 2004); there are several premotor elements active in afferent stimulus experiments.

We used intracellular depolarization to examine the intrinsic response of the motoneurons. A series of current pulses of different magnitudes was injected to depolarize the motoneurons to suprathreshold potentials, and the resulting change in spike frequency was measured. To simplify the description of change in spike rate, the initial spike frequency is referred to as F1 and the later sustained frequency F2 (Fig. 4b). This distinction is based on the observation that after about 100 ms of depolarization, the spike rate becomes relatively constant for the duration of depolarization and shows no further adaptation (Chapple and Krans 2004). F2 is thus defined as the rate during the later, constant spiking period. For consistency, F1 is defined as the mean instantaneous frequency during the first 80–100 ms of depolarization. Although F1 and F2 are treated as discrete values for descriptive purposes, it is clear that they are not discrete; F1 and F2 are epochs of a continuous decay (Fig. 4c, a linear model approximates the initial spike intervals of F1, $r = 0.94$, and $P < 0.01$). Three mechanisms that might generate the spike reduction from F1 to F2, as observed in depolarization trials, are: (1) an interneuronal pathway receiving excitatory input from

◀

Fig. 2 Reflex activation of the VSMN. **a** Extracellular hook electrode recordings from a site proximal to a stimulating electrode on the first nerve of the fourth ganglion, which is primarily composed on afferents. *Gray* Average of 20 subthreshold stimuli; *black* average of 20 stimuli at 110% of threshold, indicating a single phase-locked afferent potential with no instances of multiple spikes in the average. **b** Extracellular suction electrode recording from the motor nerve (third nerve) showing the spiking pattern of several of the VSMN after a single stimulus to the afferent nerve (*arrowhead*). **c** PSDF of VSMN firing after single stimulus to the afferent nerve (*arrowhead*). *Dotted curve* Lateral VSMN, which is typically quiet in the isolated ganglion. *Dashed curve* Medial VSMN, which is spiking at about 4 Hz before stimulus. The medial VSMN shows robust activation with a single electrical stimulus of the afferent nerve (*phase 1*), followed by modest inhibition (*phase 2*), and finally an elevated spike rate (*phase 3*). *Solid curve*, the central VSMN, spiking at about 12 Hz before afferent stimulus shows a robust inhibition during phase 2, but only a small phase 1 activation, whereas phase 3 is very long and consists of elevated spike frequency. **d** Two examples of intracellular recording from the medial VSMN with single stimulus to the afferent nerve (at $t = 0$ in each panel). The top portion of each panel is the extracellular recording from the motor nerve, which depicts activity of all VSMN. The right vertical axis is instantaneous frequency. Frequency values are plotted at the midpoint between the two events used in their computation (*filled gray circles*). Proposed IPSPS are marked with *arrows*. Note the membrane potential dependent increase in amplitude of these IPSPS in the *right panel*

VSMN feeds back an inhibitory action onto VSMN. Depending on the number of synaptic connections in this Renshaw-like circuit, the action could require only a few milliseconds. Upon intracellular depolarization of the motoneurons, the onset of spike rate reduction is in dozens of milliseconds (In Fig. 4d, one example from the

▶

Fig. 3 Excitatory synaptic content of phase 1 reflex activation of VSMN. **a** Hyperpolarizing current abolishes action potentials in the medial VSMN and permits the visualization of EPSP generated depolarization characteristic of phase 1. This is an example of a single electrical stimulus to the afferent nerve (*arrowhead*). The final EPSP present during the hyperpolarizing step is not substantially different in amplitude from the spontaneous EPSPS that precede stimulus. *Inset* Magnification of the period directly following afferent stimulus. The first three EPSPS triggered by stimulus arrive with interevent intervals of: 24.0, 34.6, and 83.9 ms. These latencies are representative of data gathered across several experiments ($n = 9$) and indicate instantaneous frequencies of 41.72, 28.88, and 11.92 Hz, respectively. **b** Depicted is a recording from the hyperpolarized medial VSMN when afferent stimuli are delivered at about 15 Hz (*arrowheads*). EPSPS recorded in VSMN follow afferent stimulus to between 15 and 18 Hz, depending on the motoneuron. Repetitive stimulus of the afferent nerve yields excitatory synaptic potentials in VSMN that fall into relatively tight distributions of amplitude. **c** Histogram of the voltage deflections attained from experiments such as that depicted in panel B. Note the multiplicative relationship between the smallest amplitude distribution (*1*) and the other distributions (*2*, *3*, and *4*). The variance of each distribution is less than 10% of the mean value. Amplitudes were measured over a 1-s period and several trial repetitions, indicating that the amplitude distributions did not change with time. **d** Averaged recordings from the lateral VSMN when afferent stimuli are delivered at about 40 Hz. The initial evoked potential was always greater than the following events and the sustained membrane potential during stimulus is greater than the resting potential preceding stimulus. Hyperpolarizing current was passed in these trials to eliminate motoneurons spiking

circular VSMN is shown, $n = 13$ preparations total), (2) an intrinsic membrane current, such as the activation of a voltage-sensitive repolarizing current or calcium-activated potassium current (Grillner et al. 1995; Guckenheimer et al. 1997), and (3) though we have yet to document direct pathways to VSMN inclusive of non-spiking interneurons, it is possible that the feedback activation of such a neuron could generate the rate decay observed.

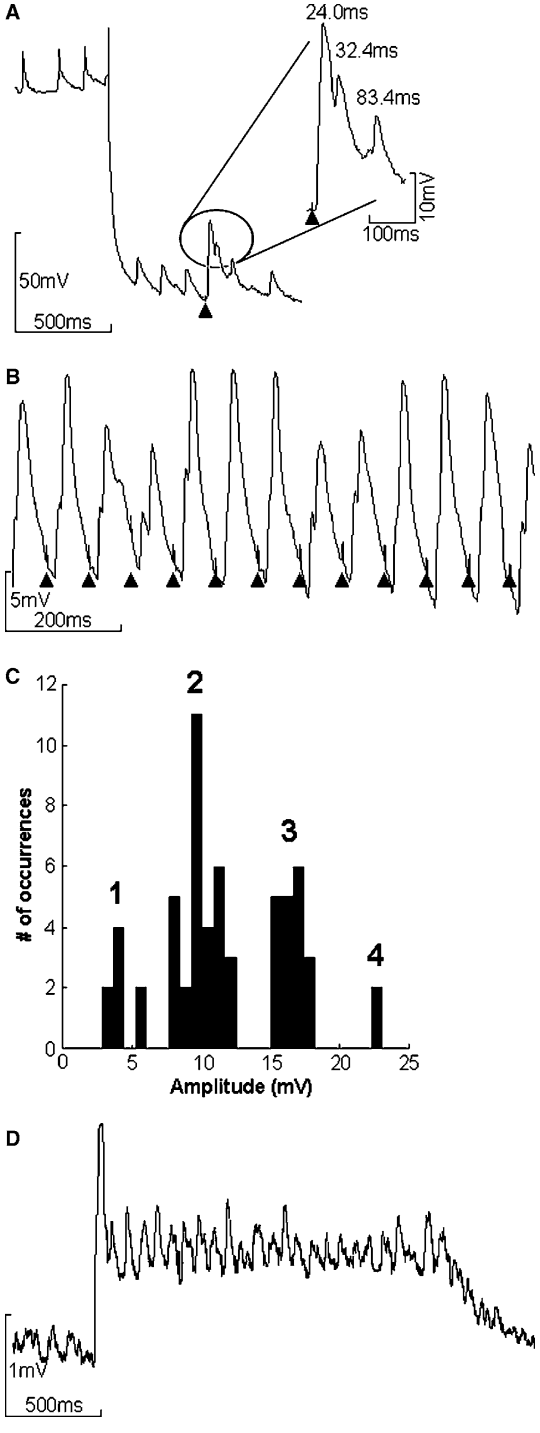

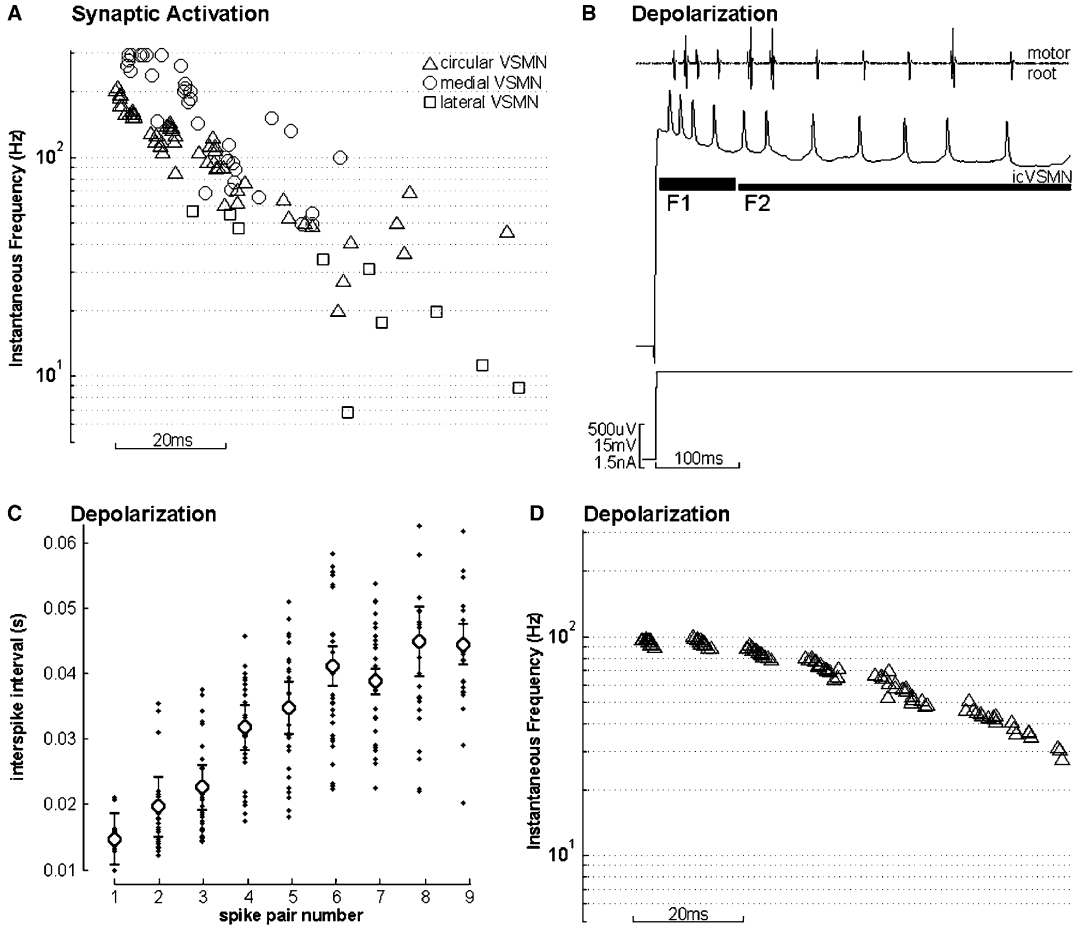

Fig. 4 The decay of spike frequency over time when activated by reflex/synaptic pathways and intracellular depolarization. **a** Instantaneous frequency of VSMN as a function of time after motoneuron activation by a single afferent stimulus (synaptic activation). The three VSMN that show the most robust firing rate during phase 1 are plotted. The decay in spike frequency is best fit by a single exponential, though deviation increases substantially with time. **b** Spike frequency adaptation from intracellular depolarization of VSMN. *Top* Extracellular recording from the motor nerve. The smallest class of potentials in the extracellular trace, the transverse VSMN, is correlated with the intracellular potentials; *Middle* Intracellular depolarization of the VSMN causes spiking that decays over time from an initial period of high-frequency spiking (F1) to a relatively steady state (F2). *Below* Magnitude of current passed for depolarization remains constant throughout the period. **c** Interspike interval is plotted as a function of spike pair number, independent of time. Spike pair number refers to two action potentials, i and $i+1$, indexed sequentially from the first spike upon depolarization. *Dots* are intervals measured from 30 trial repetitions in the transverse VSMN, *open circles* are the mean of each spike pair interval across these 30 repetitions, and *error bars* are ± standard error. **d** Instantaneous frequency (1/interspike interval values, $n=10$ trials) of the circular VSMN during depolarization by a constant magnitude current-step. The rate of frequency adaptation is not well fit by a single exponential as in **a**, but remains constant for about 20 ms, and then decays less rapidly than **a**

The decay from early to late spike rate was always smooth; there was no indication of discontinuity in any of the depolarization magnitude sampling intervals (i.e. Fig. 4). This is in contrast to an abrupt change that would support an interneuronal feedback hypothesis. The magnitude of adaptation was lesser in trials of depolarizing current than in afferent stimulus trials (whereas data of Fig. 4a could be well fit with either first or second order exponentials: F test, $P<0.01$ both; neither of these functions approximated the data of Fig. 4d well, $P>0.05$). For example, over the initial 50 ms of synaptically activated reflex spiking, the circular VSMN decreased in firing rate from about 110 to 30 pps, whereas the adaptation from depolarization alone was from about 95 to 50 pps (Figs. 4a, 3d; ratio of last instantaneous frequency to first instantaneous frequency = 0.27 and 0.53, respectively, $P<0.01$).

As the depolarizing current magnitude was increased, motoneuron spike rates during F1 and F2 also increased (Fig. 5a). As the depolarizing current magnitude was increased, there was a point at which little to no increase in spike rate in either the early or late epochs occurred. This magnitude differed from preparation to preparation, possibly as a function of the intracellular penetration site. F1 approaches this maximum frequency more rapidly than F2, but F2, as a proportion of F1, increased by only a small amount across a wide range of current magnitudes. The slight increase in this ratio is caused in part by the saturation of F1, while F2 continues to grow over the same range of currents. Figure 5b depicts this relationship for the two VSMN that contribute most to

longitudinal force in the abdomen, the medial and lateral motoneurons. The mean lateral VSMN F2:F1 value was 0.23 ± 0.014 (error = 6.2% of the mean), and the slope of the linear best-fit line was 0.022 ($r = 0.95$). F2:F1 computed from the medial VSMN spike rate had a greater rate of change with the magnitude of depolarization than that of the lateral VSMN: slope = 0.068 ($r = 0.95$, χ^2 $P < 0.01$). Its mean and standard error were also greater: mean = 0.48 ± 0.039 (error = 8.31% of the mean). These values are representative of ratio-current relationships computed across many preparations (medial: $n = 5$ preparations, lateral $n = 4$ preparations). The (F2:F1)-current relationship (Fig. 5b), which was computed from the data of Fig. 5a, for each experimental series and VSMN was used as a template in the process of evaluating changes in the spike rate decay phenomenon.

Intrinsic or extrinsic mechanism

If F2:F1 were dependant on inhibitory synaptic input, then its value should increase when synaptic pathways are attenuated, providing a way of distinguishing between presynaptic and intrinsic mechanisms of adaptation. In contrast, if the rate reduction were dependant on intrinsic membrane currents, then F2:F1 should not change when the nerve cord is exposed to saline that interrupts synaptic pathways. Saline containing an elevated calcium and magnesium concentration (HCM) was used to reduce the contribution of polysynaptic pathways. HCM saline has been used previously in both vertebrate (Parker 2003) and invertebrate species such as crayfish as well as hermit crab [crayfish: (Le Bon-Jego and Cattaert 2002); hermit crab: (Chapple and Krans 2004)]. In a recent report, Parker showed that HCM effectively blocked delayed IPSPS (average delay ~ 20 ms) of a feedforward motoneuronal circuit in lamprey (2003). This result is of particular value to our investigation as we are employing the saline as a means to reduce presynaptic inhibitory elements involved in a feedforward reflex system.

High Ca^{2+}, high Mg^{2+} Cole's saline reduces spontaneous synaptic events recorded intracellularly from VSMN of a physically isolated ganglion by approximately threefold, and completely abolished visible IPSPS. In one experiment, the rate of occurrence of post-synaptic potentials (both excitatory and inhibitory) was 5.67 ± 0.21 Hz in Cole's, and 1.91 ± 0.067 pps in HCM (excitatory only). The spontaneous post-synaptic potential rate reversed to 5.2 ± 0.23 pps when HCM was washed out with normal saline. Polysynaptic activation of the VSMN was reduced substantially in ganglia bathed with HCM but monosynaptic activation—via afferents—persisted (Figs. 5c, 4d; afferent pathways: Chapple 2002; Chapple and Krans 2004). HCM saline did not significantly alter membrane resistance; small hyperpolarizing currents were passed intracellularly and the voltage deflections measured as an indication of changes in membrane resistance. In one experiment, the mean voltage deflection from a 0.5 nA hyperpolarizing pulse was: in Cole's: -5.23 ± 0.41 mV and in HCM: -5.36 ± 0.12 mV (Fig. 5e, t test, $P > 0.05$, $n = 7$ preparations total, 30 repetitions each). The potential to which the VSMN membrane was depolarized and the amplitudes of action potentials recorded intracellularly were similar in Cole's and HCM (Fig. 5f). Though F1 and F2 increased in HCM when compared to similar current magnitudes in Cole's saline (Fig. 5a), F2:F1 ratio values did not change significantly (Fig. 5b, ANOCOVA, lateral: $P = 0.45$, medial: $P = 0.88$). This suggests that synaptic events are not critically involved in the spike frequency adaptation observed.

Experiments using HCM saline were duplicated using a low Ca^{2+}, high Mg^{2+}, Mn^{2+} saline (LCHM, Swensen et al. 2000) to evaluate previous results in preparations with further reduced synaptic activity. This saline abolishes or substantially reduces all synaptic pathways (Parker and Newland 1995; Wachowiak and Cohen 1998). Figure 5c and d illustrate the action of LCHM on phasic activation of VSMN; there are no mono or polysynaptic potentials visible in intracellular recordings from VSMN bathed in this saline. Spontaneous VSMN spiking was reduced with time in LCHM, as were intracellularly recorded spike amplitude deflections ($n = 3$ preparations). We were unable to drive VSMN across an equivalent range of frequencies between Cole's and LCHM application. For the range of F1 frequencies that was similar in Cole's and LCHM saline, there was no difference in the F2:F1 ratio computed from data gathered in Cole's saline and that from LCHM (χ^2 statistic, $P > 0.05$). In one experiment, F2:F1 in the medial VSMN was 0.44 ± 0.016 in Cole's saline and 0.42 ± 0.011 in LCHM saline. These results support the hypothesis that the mechanism of spike rate reduction is intrinsic to VSMN.

Time course and voltage/frequency sensitivity

The duration of phase 1 is sometimes very brief (only dozens of milliseconds) and this raised the question: does the spike frequency adaptation occur with brief activation? Latency to onset of spike frequency adaptation was investigated using an intracellular current injection protocol ($n = 7$ preparations). This consisted of a variable duration but brief depolarizing step of current (I_1), a 75 ms cessation of current injection (I_2), and finally a second depolarizing step of a longer duration (I_3, Fig. 6a). The metric used in these experiments was the ratio F1′:F1, where F1 was defined as the VSMN spike frequency during the initial depolarizing current injection, and F1′ was the frequency computed from the first 80 ms of the second depolarizing pulse (Fig. 6a). Thus, upon activation of the adaptation mechanism the ratio F1′:F1 would decrease. Figure 6b shows that F1′:F1 decreases over the first 20–30 ms and then approaches a steady value for longer initial depolarizing pulses.

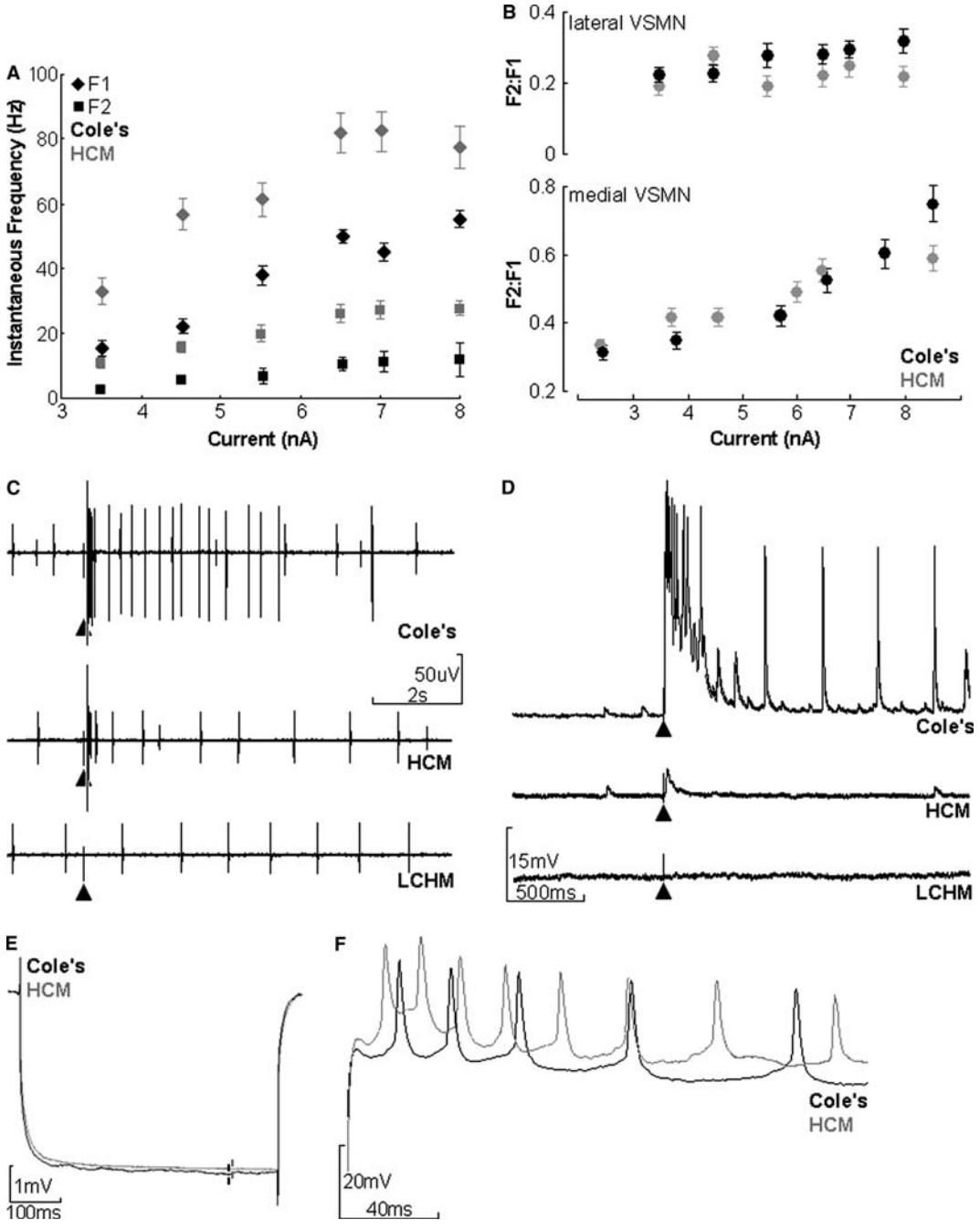

F1′:F1 values computed from I_1 durations of less than 20 ms were greater than those computed from I_1 values greater than 20 ms (ANOVA, lateral: $P = 0.02$, medial $P < 0.01$). This suggests that the mechanism responsible for rate reduction increases in efficacy during the initial 20–30 ms of depolarization. In all experiments of this design, F1′:F1 computed from trials with initial depolarization duration ≥30 ms was roughly equivalent to the ratio F2:F1 computed from single-pulse trials for a given VSMN (Fig. 5b).

The action of spike frequency adaptation, initiated during phase 1, on the later phases remained unclear; could the adaptation persist through the repolarization of phase 2 and act on the spike rate of phase 3? We observed that two equivalent depolarizing current steps, when within a few seconds of one another, always yielded a lesser spike frequency in the later depolarization than the first ($n = 6$ preparations). This indicates that the adaptation mechanism remains active after the termination of VSMN depolarization and spiking. Figure 6c illustrates the protocol of current steps used to characterize this. The duration of the first depolarizing current pulse was constant and sufficient in duration to activate the mechanism (I_1, 100 ms). The second period was a variable duration repolarization to resting membrane potential (I_2). Finally, a depolarizing current pulse, of

◀

Fig. 5 The F2:F1 relationship, a measure of spike frequency adaptation, in Cole's saline, an elevated calcium and magnesium saline (HCM), and a low calcium, high magnesium saline (LCHM). **a** Instantaneous frequency as a function of current magnitude. F1 (*diamonds*) and F2 (*squares*) grow at different rates with current magnitude (*f–I* relationship). *Black symbols* Frequency data collected while the ganglion was bathed in Cole's (normal) saline. *Gray symbols f–I* relationship from the same cell (lateral VSMN) now in HCM saline. Although HCM frequencies are significantly greater than those in Cole's saline, the ratio F2:F1 remained the same. This relationship is depicted in **b**. *Top* F2:F1 ratios from the lateral VSMN, computed from the data shown in **a**. There is a slight increase in F2:F1 as current increases, but no significant change in this relationship between Cole's and HCM saline. *Below* Similar data, collected from the medial VSMN. The medial VSMN F2:F1-current relationship has a steeper slope than that computed for the lateral VSMN. There was no difference between HCM data and Cole's data for the medial VSMN. **c** Extracellular recordings from a motor nerve of one preparation bathed in Cole's, HCM, and LCHM. *Top* Control activation by a single afferent stimulus (*arrowhead*) in Cole's saline; the second largest amplitude is the medial VSMN. *Middle*, the same preparation and stimulus intensity with the ganglion bathed in HCM. The lateral VSMN fires a single action potential, but the medial VSMN amplitude is absent. *Bottom*, equivalent stimulus, same preparation, while the ganglion is bathed in LCHM. No phasic activation of VSMN is present. **d** Intracellular recordings from the medial VSMN corresponding to the experiments in panel C (timescales in **c** and **d** are not equal). **e** Average of voltage deflections to a 0.5 nA hyperpolarizing step, 20 trials each. There was no change in the voltage deflection between Cole's saline (*black*) and HCM (*gray*) in any of the VSMN. Standard error is plotted as vertical lines at about $t = 400$ ms. **f** Intracellular depolarization of the medial VSMN in Cole's (*black*) and HCM (*gray*) saline. The same magnitude of current was used in each trace. There is a substantial increase in spike frequency while the ganglion is bathed in HCM and a slight increase in voltage deflection (to a more depolarized potential)

the same magnitude of the initial depolarization, was passed for a fixed duration of about 600 ms (I_3). The duration of repolarization was varied to determine the time at which the I_3 depolarization would generate a VSMN spike rate similar to that observed from I_1 depolarization. Figure 6d shows that the value F1′:F1 grows with the duration of the repolarization period (I_2). These data are well fit by a second order logarithmic function (F test, $P < 0.01$). The transient repolarization produces an increase in F1′ over its value in the absence of repolarization, though this increase never restored the initial excitability of the motoneuron (F1′ = F1). In the medial VSMN, F1′:F1 was 0.78 ± 0.016, computed from experiments with a 500 ms pause duration (I_2). This increase in F1′:F1 ratio is a substantial increase (~70%) over F2:F1 computed from continuous depolarization trials (0.48 ± 0.0058). In this series of experiments, the pause duration was extended to 1200 ms with no significant increase in F1′:F1 over the 500 ms duration values (data not shown). About 67% of the initial VSMN excitability is regained after repolarization to rest for about 250 ms (tau $F1':F1_{max} = 242 \pm 14$ ms).

As the underlying EPSPS of phase 1, and those of phase 3 are variable in time and rate (Fig. 3; Chapple and Krans 2004), we were interested in the action of depolarizing current on the parameters of spike frequency adaptation. The rate at which VSMN spike frequency adapts is a function of depolarizing current magnitude. We varied the magnitude of depolarization and measured the time required for a reduction of spike rate of about 63% from peak initial frequency ($n = 7$ preparations). All data from these experiments were normalized in two ways: (1) instantaneous frequency was normalized to the maximum value within each set of repetitions, which was usually the frequency computed from the first pair of action potentials upon depolarization, (2) the time of the first interspike interval was set to zero. Three magnitudes of depolarization from a single intracellular experiment are shown in Fig. 7a ($n = 10$, each magnitude). These data illustrate the change in tau with increased current (F test for multiple populations; 7 nA versus 3.5 nA: $P < 0.01$, 3.5 nA versus 4.5 nA: $P < 0.01$, but 7 nA versus 4.5 nA: $P = 0.98$). Figure 7b shows this quantitatively: the time constant of spike rate decay increased as a function of depolarizing current magnitude (linear, $r = 0.70$).

As the magnitude of depolarization increased, so did the duration of the high-frequency early period ($n = 7$ preparations). Figure 7a illustrates this graphically. Within the 7 nA data set (solid squares), there are two clusters of data at similar mean frequencies that occur within the first 20 ms of depolarization (open arrowheads: $96.16 \pm 0.20\%$ and $95.79 \pm 0.48\%$ of normalized scale). In contrast, the 3.5 nA data set (gray triangles) has only one cluster at the peak-normalized frequency, indicating that decay in rate began sooner for this lower magnitude of depolarization. These observations might be expected from single electrode current injection to a site distant from the spike initiation zone. This longer period of high-frequency spiking may be partially responsible (~10 ms shift) for the robust increase in tau as current increased, as plotted in Fig. 7b. The positive linear relationship persisted in experiments where the duration of F1 did not change greatly.

To investigate voltage sensitivity of the recovery from adaptation, we used another three-pulse protocol. Figure 7c illustrates the protocol, the properties of which were: (1) the first depolarizing step (I_1) was set to a constant 80 ms duration and was relatively small in magnitude. The magnitude of this depolarization was set to the magnitude necessary to drive VSMN spiking between 30 and 50 pps over the initial period, (2) the second current step (I_2) was 100 ms in duration. This step was either a further depolarization or a repolarization and consisted of eight different magnitudes per experiment (Fig. 7c). We chose relatively small current deflections (ΔI) in an effort to limit error originating from unknown membrane charging constants, and (3) the final current step (I_3) was a return to the current magnitude of the first step ($I_3 = I_1$) for 600 ms. The ratio F1′:F1 was used to examine changes in spike rate reduction (Fig. 7c). If the mechanism responsible for rate reduction is voltage sensitive, then F1′:F1 should be determined by the transient I_2 current rather than the

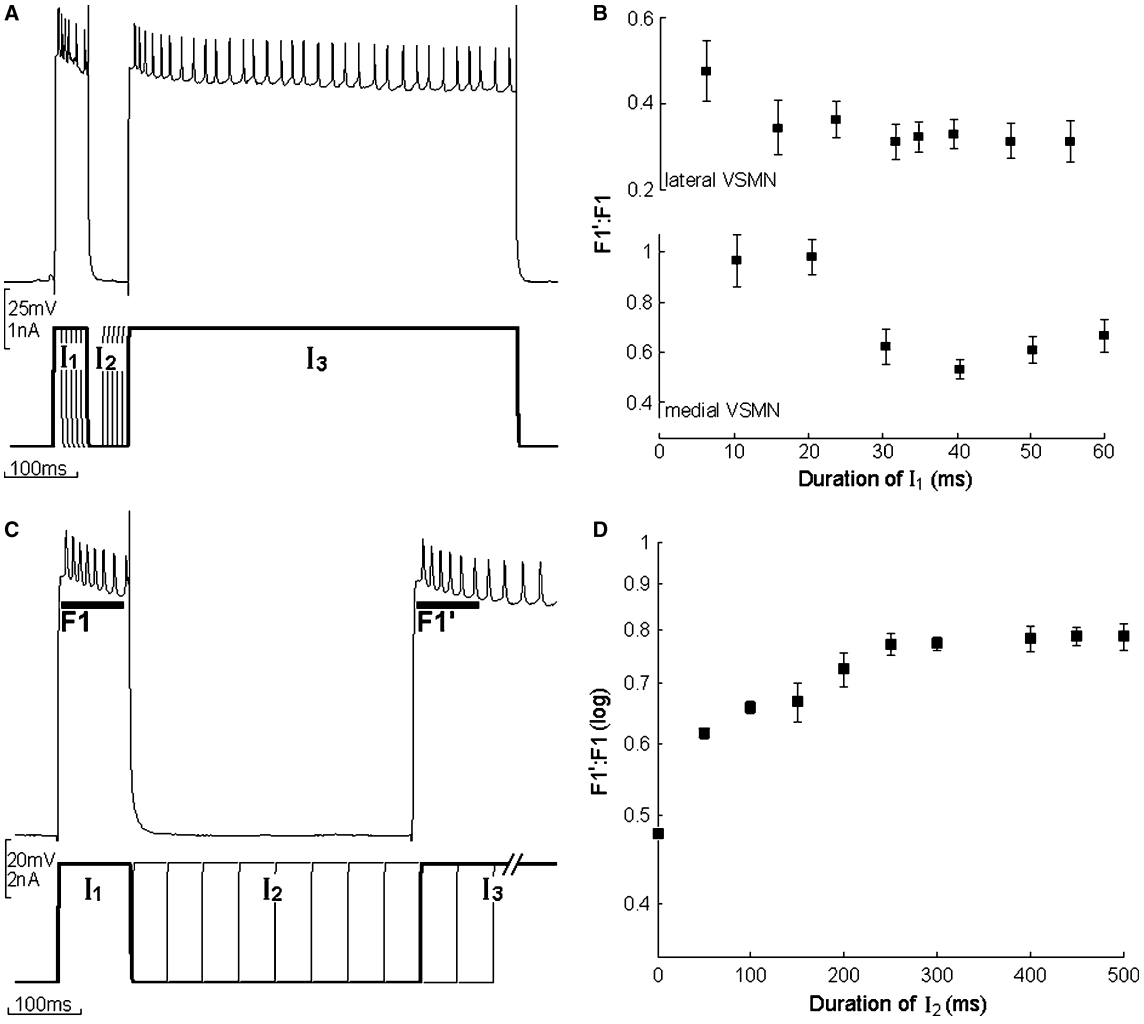

Fig. 6 Characteristics of VSMN spike frequency adaptation in time. **a** Experimental protocol for the investigation of latency to onset of the spike rate reduction mechanism. *Top* Intracellular depolarization of medial VSMN. Spiking during the first depolarization step (I_1) was termed F1, as in previous experimental designs. The first 100 ms of the second depolarization (I_3) are termed F1′, which can be compared to F2 values from experiments of single long-duration depolarization. *Bottom*, *thick* Current trace used in the example shown above. *Thin* Variations in the time domain followed these outlines, with a minimum of ten repetitions for each time. The repolarization period (I_2) was always 80 ms so that the second depolarization (I_3) occurred at a fixed time after the cessation of the first. **b** *Top* Data from experiments depicted in **a**. F1′:F1 in the lateral VSMN decays rapidly to a nearly steady state with initial depolarization periods of greater than about 20 ms. *Below* In the medial VSMN, the ratio F1′:F1 remained at values of about 1 until an I_1 duration of 30 ms or greater, at which point it dropped to values normally observed from the medial VSMN. **c** Experimental protocol for the investigation of duration of the spike rate reduction mechanism upon repolarization. The epochs F1 and F1′, and current-steps I_1, I_2, and I_3 are defined in a way similar to **a**. In these experiments, the duration of I_1 was fixed at 100 ms, but the period between the first and second depolarization (I_2) was varied. Data from these experiments are plotted in **d** F1′:F1 does not return to a value of 1 with inter-depolarization pauses as long as 500 ms. The increase in F1′:F1 with time is a smooth function with little variation

initial I_1 current. We hypothesized that I_2 current magnitude values less than I_1, transient repolarization, would attenuate the rate reduction mechanism (Fig. 6d) and that F1′:F1 would increase. Similarly for I_2 values greater than I_1, VSMN membrane potential would be more depolarized, and we hypothesized that the rate reduction mechanism would be augmented, decreasing F1′:F1. This relationship is confirmed by the results depicted in Fig. 7d, which illustrate the dependence of the ratio F1′:F1 on ΔI ($n = 3$ preparations, ANOCOVA, $P = 0.001$). During continuous depolarization at the current magnitude of I_1 and I_3, F2:F1 was 0.51 ± 0.013.

The results of this experiment also serve as further evidence that the rate reduction phenomenon is not dependant on an interneuronal feedback pathway. As I_2 is the subthreshold for initiating an action potential, no synaptic interneuronal feedback could occur; no VSMN spikes are present to drive an inhibitory interneuron (Fig. 7c). If feedback were essential for rate reduction, then the relationship between F1′:F1 would be constant over this range of I_2. This was not the case; throughout the subthreshold range ($\Delta I = -0.5$ to -3.0 nA), there is

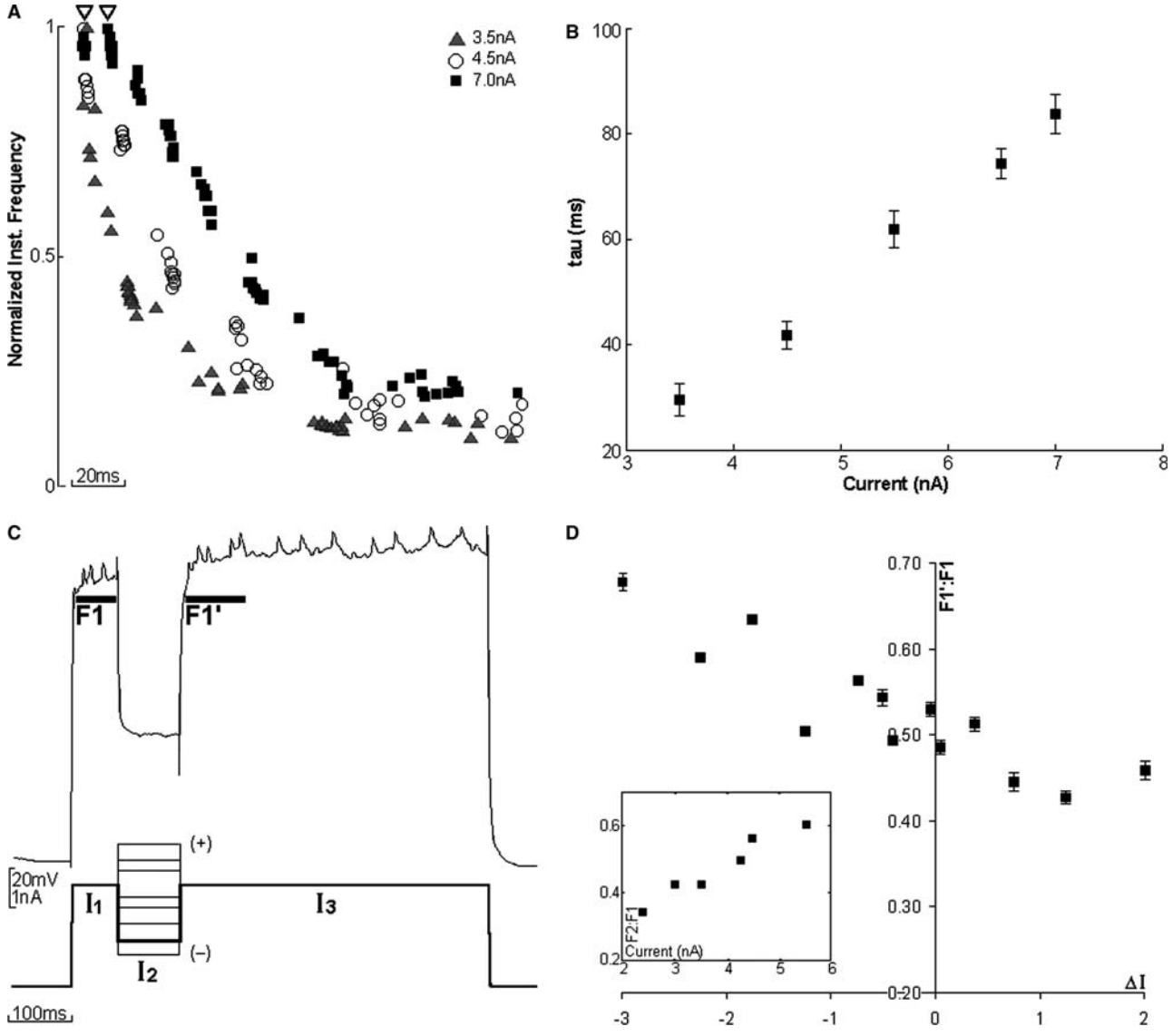

Fig. 7 Sensitivity of the spike frequency adaptation to changes in current magnitude (as an approximation of membrane voltage). **a** Normalized instantaneous frequency as a function of time. Three examples of current magnitude that represent the minimum, an intermediate value, and the maximum magnitudes passed are shown (these data from the medial VSMN). *Open arrowheads* Two clusters of instantaneous frequency from the 7.0 nA data set (*squares*), referenced in text. The time to about 63% of maximum instantaneous frequency (tau), from several current magnitudes, is plotted as a function of current magnitude in **b**. Values of tau increase in a positive relationship with current magnitude. **c** Experimental protocol for the investigation of voltage sensitivity. The current magnitude of I_1 always equaled that of I_3. I_2 was varied in polarity and magnitude. The duration of each current step was constant for all trials and repetitions. The epochs F1 and F1′ were defined as in previous experimental designs. When computing ΔI, values of I_2 greater than I_1 and I_3 were considered positive (+) deviations and when I_2 was a lesser current magnitude than I_1 and I_3, the deviations were considered negative (−). Results from these experiments are plotted in **d**. *Inset* Data from the medial VSMN depicted in Fig. 4b, for comparison with data in **d**. Varying the magnitude and polarity of the current-step I_2 led to F1′:F1 values that were a function of ΔI (I_2-I_1) rather than I_1 alone, such that increases in I_2 led to proportionate decreases in F1′:F1 and vice versa. This is in contrast to data collected from the same cell using single long-duration current steps (*inset*)

a robust and significant relationship between ΔI and F1′:F1 ($r=0.89$, $P<0.01$). While it is possible that an electrotonic junction is involved in such a feedback pathway, the latency-to-onset results (Fig. 6b) suggest that there must also be at least one chemical synapse involved; electrotonic junctions alone are too rapid to account for a latency in the dozens of milliseconds in a physically isolated ganglion (Phelan and Starich 2001). Thus, results from intracellular investigations of the postural motoneurons suggest that the mechanism for spike rate adaptation is intrinsic, its onset is within the initial 20 ms of depolarization, over the first 100 ms of depolarization spike rate is reduced between 50 and 80%, and that these parameters are sensitive to variations in the magnitude of depolarization.

Contribution to force

Spike rates observed during both the synaptically evoked and intracellularly applied current regimes of phase 1 fall

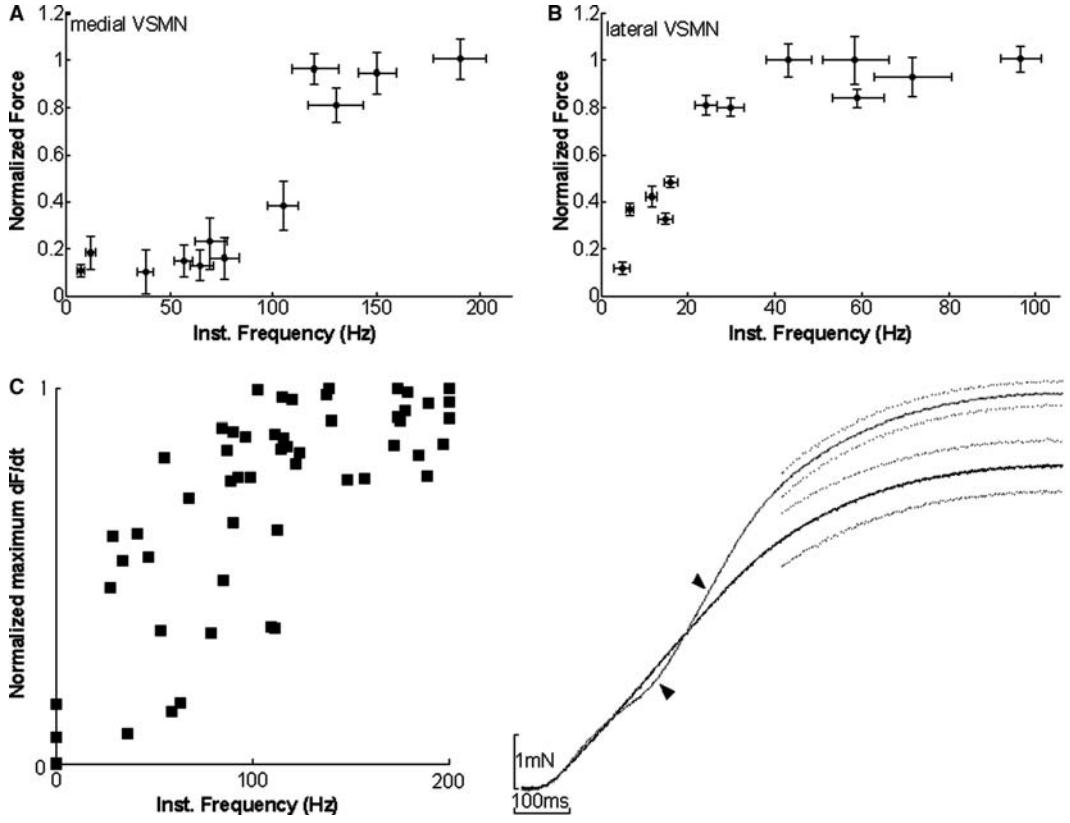

Fig. 8 The impact of spike frequency adaptation on longitudinal force. **a** Normalized longitudinal force as a function of instantaneous firing frequency. Data were collected from 100 ms steps of depolarization to the medial VSMN over several experiments while other VSMN were not active (n = 6 preparations). Forces are normalized to the maximum value observed in trials of this experimental design. **b** as in **a**, but data were gathered from the lateral VSMN, which innervates spiking muscle fibers (n = 4 preparations). **c** Normalized peak d F/d t as a function of instantaneous frequency from the medial VSMN ($r = 0.68$, F test, $P < 0.01$). **d** Averaged force traces, *Black* Continuous depolarization of VSMN for approximately 600 ms; *Gray* Force generated by the 3-pulse current magnitude protocol, with repolarization during I_2, also 600 ms in duration. *Light gray* Standard error about each averaged trace ($n = 10$ each, χ^2 test, $P < 0.01$). The pause inherent to the three-pulse protocol yielded a transient reduction of force and the later increase in frequency (F1′) yielded a transient increase in force production (*arrowheads*)

onto an area of the rate-force curve of VSM that results in rapid force recruitment. Figures 8a and 8b show the relationship between VSMN spike rate and force for the two VSMN that contribute most to longitudinal force: the medial and lateral VSMN. The central, medial, and lateral VSMN contribute about 10, 35, and 55% of the total longitudinal force generated by direct stimulus of the motor root, respectively (data not shown). The contribution of each longitudinal muscle group varied widely between preparations. This can be attributed to changes in total muscle area and the relative area of each muscle group (i.e. lateral : medial : central) as well as dynamics that are dependent on seasonal variations, the molt cycle, and small variations in the abdominal mechanics from animal to animal. The circular and transverse muscle groups were excluded from this analysis because neither of these is oriented purely longitudinally along the abdomen. The data of Figs. 8a and 8b were gathered by passing a series of 100 ms depolarizing current steps to VSMN such that the spike rate was relatively constant within each step but was varied across the series. HCM was bathed over a single ganglion within a hydrophobic well, physically distinct from the saline surrounding the muscle. This was done to eliminate spontaneous activity from VSMN of that ganglion so that the spike rate of a single VSMN, and the impact of that rate on force, could be considered without confounding spiking from other VSMN.

We hypothesize that the reduction in spike rate observed during phase 1 of reflex activation reduces peak force by limiting the initial period of muscle activation. This hypothesis implies that a continuous spike rate similar to the initial values recorded in afferent activation trials would generate forces much larger than those normally observed during reflex activation. A mean spike rate of 150 pps for 100 ms from the medial VSMN (e.g. Fig. 4a) generates about 95% of maximum force in the medial muscle fibers (Fig. 8a, $n = 6$ preparations). Similarly, the lateral VSMN spiking at 60 pps (e.g. Fig. 4a) for 100 ms produced greater than 95% maximum force in the lateral muscle fibers (Fig. 8b, $n = 4$ preparations). Spike rates early in the F1 epoch were always above the frequency necessary to generate 95% of the total force.

A second consequence of the short duration high-frequency burst during phase 1 is that the rate of force generation rapidly approaches a maximal value during

reflex activation and depolarization trials. Figure 8c shows the relationship between the derivative of force and medial VSMN spike rate. Data shown in Fig. 8c were gathered by depolarizing the medial VSMN in the absence of other motoneuron activity so that the only contribution to longitudinal force was the medial VSMN, which was depolarized for 100 ms. The mean spike rate over this period was computed for several depolarizing current magnitudes ($n = 9$ preparations). d F/d t was normalized to the greatest value observed from maximum depolarization trials to provide a ratio of observed force generation rate to the maximum possible (Fig. 8c). These results support that the initial motoneuron spike rate of phase 1, if not reduced by intrinsic spike frequency adaptation, is sufficient to generate maximum force.

To confirm this, force generation by a short constant frequency burst of spikes was compared with a burst in which frequency decreased due to adaptation. By interjecting a brief repolarization of the membrane during depolarization, a current step generated a more constant VSMN spike frequency than did a continuous depolarization (e.g. Fig. 7d). The three-pulse protocol described in relation to Fig. 7c (3 pulse) was employed in experiments with the fourth segment of ventral superficial muscle and motor root intact ($n = 3$ preparations). Longitudinal force values gathered from the two experimental designs, continuous and discontinuous depolarization, were examined in the medial VSMN; its f–I relationship was most favorable for controlled spike frequencies elicited by relatively small current magnitudes. The range of VSMN spike rate investigated within each of the two experimental designs was equivalent (60–120 pps). The critical result of these experiments is summarized in Fig. 8d, which is a comparison of the mean force produced by the 3-pulse protocol (Fig. 7c)—approximating constant spike rate—and the mean force produced by continuous depolarization trials—representing normal spike rate decay. Data from the two experimental designs were grouped by similar initial spike rate. Peak longitudinal force was greater in trials of pseudoconstant spike rate than in those with normal rate decay ($n = 40$ trials, t-test, $P < 0.01$). In the example shown, the 3-pulse force trace (gray) was generated by an average spike rate of 81.045 ± 1.71 pps during the first 100 ms, which decayed to 51.19 ± 0.51 thereafter (F1′:F1 = 0.63). The force trace from normal spike rate decay experiments (black: continuous depolarization) was generated by a VSMN spike rate that began at 88.30 ± 1.70 pps and decayed to 42.65 ± 1.12 pps thereafter (F2:F1 = 0.48). These results indicate that the reduction in spike rate that is generated solely by intrinsic mechanisms has a significant effect on force production.

Discussion

The stereotyped pattern of reflex activation of postural motoneurons in the abdomen of the hermit crab consists of three phases, an initial high-frequency burst, an interruption of motoneuron firing, and a lower frequency after-discharge lasting for several seconds (Figs. 2b and 2c). Intrinsic membrane properties of the motoneurons play a major role in the transition between the first and second phase; the resulting spike frequency adaptation acts to limit force production during the first phase of reflex activation. Variation in the magnitude of this adaptation over short periods significantly alters total force and rate of force production. Although phase 1 generates a rapid increase in force, previous investigations in intact animals and reduced preparations have shown that the total force generated by the reflex is not maximal. Reflex-generated forces are typically less than 20% of the maximum force generated by direct stimulation of the motoneuron axons (Chapple 1997; Chapple and Krans 2004). Thus, the termination of the high-frequency phase and the subsequent pause and lower frequency after-discharge is an essential element of the reflex, resulting in a rapid elevation of muscle force to a submaximal level. While it was initially proposed (Chapple 1997) that modulation at the mechanoreceptor-motoneuron synapse was the primary origin of the termination of phase 1 and the resulting rapid, but controlled recruitment of force, the present experiments suggest that motoneuron intrinsic properties play an important role.

There are several mechanisms that could result in the termination of the initial depolarization of the motoneurons. One possibility is that the mechanoreceptor afferents themselves fire only briefly. A single afferent spike can produce all three phases of the reflex. Ongoing stimulus to mechanoreceptors produces a sustained train of afferent action potentials that persist into the period of the after discharge (Chapple and Krans 2004). The phase 2 period of inhibition, lasting for as long as several hundred milliseconds, persists even in these conditions of relatively continuous afferent input to VSMN. Thus, the three phases of motoneuron firing are not produced by variations in afferent frequency.

A second mechanism that might produce a reduction in motoneuron frequency is a reduction in the amplitude of the afferent EPSPS. The EPSPS of phase 1 arrive closely in time (Fig. 3a) and decrease in frequency from an initial instantaneous frequency of about 50 pps to tonic rates of about 5 pps during the period of the after-discharge (phase 3). The amplitudes of the compound EPSPS fall into discrete groups that approximate multiples of a single value (Fig. 3c). If there were significant changes in the number of transmitter quanta released, EPSP amplitudes would likely show a more continuous distribution. Thus, we do not have evidence for a substantial presynaptic decrease in EPSP amplitude during the later portions of the burst period. This is in contrast to the case of depressing amplitude EPSPS in Aplysia, which reduce motoneuron rate over initial activation periods (Phares et al. 2003). These depressions in EPSP amplitude occur over periods much longer than the initial burst in *Pagurus*; the latency to amplitude

reduction is typically greater than 100 ms in Aplysia (Phares et al. 2003).

Inhibitory post-synaptic potentials are frequently observed at the end of phase 1 suggesting that they play an important role in the termination of phase 1 and the subsequent pause in firing of VSMN. The IPSPS appear during a period of nearly maximal d F/d t values (Figs. 2, 8). Because reflex generated IPSPS can transiently abolish VSMN spiking, they are temporally positioned at a critical time in the control of force. Varying the timing of these IPSPS would therefore be a strong source of modulation of the final output from reflex activation. We have yet to systematically examine the action of these IPSPS on rate reduction in the context of the tri-phasic reflex. They are likely interacting in a dynamic fashion with both the intrinsic frequency adaptation and the extrinsic synaptic transition from phase 1 EPSPS to phase 2 IPSPS. We conclude that both intrinsic spike frequency adaptation and synaptic processes act to reduce VSMN spike frequency and force production at the end of phase 1.

We do not know as yet the relative contributions of intrinsic conductances and synaptic inhibition in rate reduction. A limitation of our recording arrangement is that the site of spike initiation as well as the origin of synaptic potentials is electrotonically distant from the recording site. Thus, voltage clamp of these areas of the motoneuron membrane during the time course of adaptation has not been feasible. As in many other arthropod neurons, the soma is electrically silent, and intracellularly observed action potentials are usually no more than 10–15 mV in amplitude. The tip of the microelectrode was placed in the region of neuropil that contains the dendrites and integrating segment of the neuron, so that a current step would be filtered by the RC properties of the membrane. We have been able neither to space clamp the postural motoneurons nor to assess the resultant voltage deflections in dendrites and the integrating segment to the injection of current.

We speculate that one of two ionic mechanisms is responsible for the spike frequency adaptation: (1) a potassium current such as K_{Ca}, which is activated by the accumulation of Ca^{2+} during the period of the initial rapid spiking and depolarization, or (2) an inactivation of Na^{+} channels. The present results do not allow us to distinguish between different ionic mechanisms. It is difficult to evaluate changes in spike frequency adaptation magnitude across trials in which salines with varied Ca^{2+} concentrations were applied. Though qualitative, it is clear that spike frequency adaptation persisted in low Ca^{2+} saline. As mentioned, equivalent depolarizing current magnitude in LCHM and Cole's did not yield equivalent spike rates. As in other preparations, spike frequency adaptation is dependent upon the number and rate of spikes, it is difficult to provide a direct comparison of the adaptation in these treatments. HCM saline was more benign than LCHM (Fig. 5c and 5d, and corresponding text) and in HCM, the elevated Ca^{2+} did not substantially modify spike frequency adaptation, suggesting that this cation is not critically involved in the process. Further investigation of the biophysical properties of the motoneurons is necessary to isolate the contributing membrane current(s).

A plausible function for the tri-phasic pattern of firing may be associated with the properties of the muscle. Slow arthropod muscles are activated by graded depolarization rather than by action potentials. A prominent feature of arthropod neuromuscular junctions is a pronounced facilitation in the amplitude of the junction potentials during a train of stimuli (Atwood 1967). EJP amplitude is dependent upon the potential rate and duration of motoneuron action (Jorge-Rivera et al. 1998; Msghina et al. 1998; Zucker and Regehr 2002), and force is dependent upon total muscle depolarization (Atwood 1967). Thus, the initial burst rapidly facilitates the rate of increase in force, as has been known for many years in mammals (Buller and Lewis 1965). However, we believe that the rapid decrease in the frequency and eventual transition to phase 2 cessation of firing observed in hermit crab is unusual.

We used the 3-pulse experimental design (Fig. 7c) to compare the force resulting from relatively constant frequency spike trains to that resulting from a normal decay in spike rate. This experimental protocol permitted the reproducible control of late frequency (F2) relative to early frequency (F1′:F1 as a model of F2:F1) via the modulation of duration and intensity of the repolarization phase, I_2. Two principal results that support the hypothesis that the rate decay of phase 1 is essential to the reflex production of a stable sub-maximal force are: (1) a pause in VSMN spiking (during transient inhibition: $I_2 = 100$ ms) was necessary to produce a partial recovery from adaptation and, thus, an increase in the later spike frequency. This pause led to a transient reduction in d F/d t and then a post-repolarization increase of d F/d t to greater values than those generated in normal frequency adaptation trials, (2) although repolarization during I_2 never resulted in a total recovery from adaptation, the F1′:F1 ratio never reached or exceeded 1 (e.g. about 0.75 in Fig. 6d); the final force generated was always greater than that observed during normal frequency adaptation. In both cases, the transient repolarization might have generated a lesser final force value, but the opposite result was observed. These results strongly support the hypothesis that the decay in motoneuron spike rate during the initial period of activation is a mechanism for limiting force production so that maximal values are not attained.

In contrast to a number of rhythmic preparations in which the intrinsic properties of motoneurons have been studied, the VSMN are part of a tonic postural system that maintains muscle stiffness as part of the shell support system. In cyclic systems, such as the pyloric portion of the stomatogastric system, the generation of a repetitive pattern of activation of motoneurons with a fixed delay between PD, LP, and PY neurons requires mechanisms that will constrain the onset and termination of activation of each group. In contrast, in the abdomen of

the hermit crab, the tonic firing of the motoneurons must be combined with aperiodic signals from mechanoreceptors to produce a moderately elevated level of muscle tone. Adaptation does not appear to be present in the opener and closer motoneurons of crayfish (Lindsey and Gerstein 1979), or smaller homologous motoneurons in crayfish (Evoy 1977), although it is present in the largest superficial excitor (Gillary and Kennedy 1969). In some other arthropod species as well, adaptation is a feature of motoneuron activation. Schmidt et al. (2001) describe spike frequency reductions in stick insect leg motoneurons that would yield late:early rate ratios between about 0.2 and 0.6, but this adaptation is much slower in stick insect (about 500 ms) than in hermit crab (less than 100 ms, Fig. 7a). Spike frequency adaptation has been described in many vertebrate motoneurons (Granit 1970; Kernell 1965; Sawczuk et al. 1995a, b), though the behavioral implications of the adaptation is sometimes difficult to infer (Magarinos-Ascone et al. 1999). Rapid spike rate adaptation has been described in lamprey with frequency reduction percentages between about 20 and 80% (Martin 2002). The time course of spike rate reduction in lamprey is quite rapid, and similar to that reported here (Martin 2002). As in *Pagurus*, the magnitude of adaptation decreased with depolarization, and this is associated with a change in the state of the system: from quiescence to fictive locomotion (Martin 2002). Many different magnitudes and time constants of frequency adaptation in motoneurons have been reported, and these may be well suited to the particular species and behavior in which they are observed, though such an analysis is seldom provided. In *Pagurus*, the functional action of this intrinsic property is evident; force production from postural muscles of the abdomen is reduced.

Acknowledgements We would like to thank Andrew Moiseff and Elizabeth W. Kelly for their insightful discussions and helpful comments on the manuscript. We are grateful to Joseph Healy, who provided animals. This research was supported in part by NSF grant IBN-9874499.

References

Alaburda A, Perrier JF, Hounsgaard J (2002) An M-like outward current regulates the excitability of spinal motoneurones in the adult turtle. J Physiol 540:875–881

Atwood HL (1967) Crustacean neuromuscular mechanisms. Am Zool 7:527–552

Binder M, Heckman C, Powers RK (1996) The physiological control of motoneuron activity. In: Rowell L, Shepherd J (eds) Handbook of physiology. Exercise: regulation and integration of multiple systems. Oxford University Press, New York, pp 1–53

Buller AJ, Lewis DM (1965) The rate of tension development in isometric tetanic contractions of mammalian fast and slow skeletal muscle. J Physiol 176:337–354

Chapple WD (1969) Postural control of shell position by the abdomen of the hermit crab, *Pagurus pollicarus*. J Exp Zool 171:4, 397:408

Chapple WD (1973a) Changes in abdominal motoneuron frequency correlated with changes of shell position in the hermit crab, *Pagurus pollicarus*. J Comp Physiol A 87:49–64

Chapple WD (1973b) Role of the abdomen in the regulation of shell position in the hermit crab *Pagurus pollicarus*. J Comp Physiol A 82:317–332

Chapple WD (1974) Hydrostatic pressure changes in the abdomen of the hermit crab, *Pagurus pollicarus*, during movement. J Comp Physiol A 88:399–412

Chapple WD (1997) Regulation of muscle stiffness during periodic length changes in the isolated abdomen of the hermit crab. J Neurophysiol 78:1491–1503

Chapple WD (2002) Mechanoreceptors innervating soft cuticle in the abdomen of the hermit crab, *Pagurus pollicarus*. J Comp Physiol A 188:753–766

Chapple WD, Krans JL (2004) Cuticular receptor activation of postural motoneurons in the abdomen of the hermit crab, *Pagurus pollicarus*. J Comp Physiol A 190:365–377

Evoy WH (1977) Crustacean motor neurons. In: Hoyle G (ed) Identified neurons and behavior of arthropods. Plenum Press, New York, pp 67–86

Gabriel JP, Scharstein H, Schmidt J, Buschges A (2003) Control of flexor motoneuron activity during single leg walking of the stick insect on an electronically controlled treadwheel. J Neurobiol 56:237–251

Gillary HL, Kennedy D (1969) Pattern generation in a crustacean motoneuron. J Neurophysiol 32:595–606

Granit R (1970) The basis of motor control: integrating the activity of muscles, alpha and gamma motoneurons and their leading control systems. Academic, London

Grillner S, Deliagina T, Ekeberg O, el Manira A, Hill RH, Lansner A, Orlovsky GN, Wallen P (1995) Neural networks that coordinate locomotion and body orientation in lamprey. Trends Neurosci 18:270–279

Guckenheimer J, Harris-Warrick R, Peck J, Willms A (1997) Bifurcation, bursting, spike frequency adaptation. J Comput Neurosci 4:257–277

Harris-Warrick RM (2002) Voltage-sensitive ion channels in rhythmic motor systems. Curr Opin Neurobiol 12:646–651

Heckman CJ, Lee RH, Brownstone RM (2003) Hyperexcitable dendrites in motoneurons and their neuromodulatory control during motor behavior. Trends Neurosci 26:688–695

Jorge-Rivera JC, Sen K, Birmingham JT, Abbott LF, Marder E (1998) Temporal dynamics of convergent modulation at a crustacean neuromuscular junction. J Neurophysiol 80:2559–2570

Kernell D (1965) Synaptic influence on the repetitive activity elicited in cat lumbosacral motoneurones by long-lasting injected currents. Acta Physiol Scand 63:409–410

Le Bon-Jego M, Cattaert D (2002) Inhibitory component of the resistance reflex in the locomotor network of the crayfish. J Neurophysiol 88:2575–2588

Lee RH, Kuo JJ, Jiang MC, Heckman CJ (2003) Influence of active dendritic currents on input–output processing in spinal motoneurons in vivo. J Neurophysiol 89:27–39

Lewis DV, Huguenard JR, Anderson WW, Wilson WA (1986) Membrane currents underlying bursting pacemaker activity and spike frequency adaptation in invertebrates. Adv Neurol 44:235–261

Lindsey BG, Gerstein GL (1979) Interactions among an ensemble of chordotonal organ receptors and motor neurons of the crayfish claw. J Neurophysiol 42:383–399

Magarinos-Ascone C, Nunez A, Delgado-Garcia JM (1999) Different discharge properties of rat facial nucleus motoneurons. Neuroscience 94:879–886

Martin MM (2002) Changes in electrophysiological properties of lamprey spinal motoneurons during fictive swimming. J Neurophysiol 88:2463–2476

Morris LG, Hooper SL (1997) Muscle response to changing neuronal input in the lobster (*Panulirus interruptus*) stomatogastric system: spike number- versus spike frequency-dependent domains. J Neurosci 17:5956–5971

Morris LG, Hooper SL (1998) Muscle response to changing neuronal input in the lobster (*Panulirus interruptus*) stomatogastric system: slow muscle properties can transform rhythmic input into tonic output. J Neurosci 18:3433–3442

Msghina M, Govind CK, Atwood HL (1998) Synaptic structure and transmitter release in crustacean phasic and tonic motor neurons. J Neurosci 18:1374–1382

Parker D (2003) Activity-dependent feedforward inhibition modulates synaptic transmission in a spinal locomotor network. J Neurosci 23:11085–11093

Parker D, Newland PL (1995) Cholinergic synaptic transmission between proprioceptive afferents and a hind leg motor neuron in the locust. J Neurophysiol 73:586–594

Phares GA, Antzoulatos EG, Baxter DA, Byrne JH (2003) Burst-induced synaptic depression and its modulation contribute to information transfer at aplysia sensorimotor synapses: empirical and computational analyses. J Neurosci 23:8392–8401

Phelan P, Starich TA (2001) Innexins get into the gap. Bioessays 23:388–396

Prather JF, Clark BD, Cope TC (2002) Firing rate modulation of motoneurons activated by cutaneous and muscle receptor afferents in the decerebrate cat. J Neurophysiol 88:1867–1879

Sawczuk A, Powers RK, Binder MD (1995a) Intrinsic properties of motoneurons. Implications for muscle fatigue. Adv Exp Med Biol 384:123–134

Sawczuk A, Powers RK, Binder MD (1995b) Spike frequency adaptation studied in hypoglossal motoneurons of the rat. J Neurophysiol 73:1799–1810

Schmidt J, Fischer H, Buschges A (2001) Pattern generation for walking and searching movements of a stick insect leg. II. Control of motoneuronal activity. J Neurophysiol 85:354–361

Swensen AM, Golowasch J, Christie AE, Coleman MJ, Nusbaum MP, Marder E (2000) GABA and responses to GABA in the stomatogastric ganglion of the crab *Cancer borealis*. J Exp Biol 203:2075–2092

Taylor JR (1982) An introduction to error analysis: the study of uncertainties in physical measurements. University Science Books, Mill Valley

Wachowiak M, Cohen LB (1998) Presynaptic afferent inhibition of lobster olfactory receptor cells: reduced action-potential propagation into axon terminals. J Neurophysiol 80:1011–1015

Zucker RS, Regehr WG (2002) Short-term synaptic plasticity. Annu Rev Physiol 64:355–405